Available online at www.sciencedirect.com
SCIENCE DIRECT®
Journal of Catalysis 220 (2003) 399–413
JOURNAL OF CATALYSIS
www.elsevier.com/locate/jcat

Kinetic modeling of pore mouth catalysis in the hydroconversion of *n*-octane on Pt-H-ZSM-22

C.S. Laxmi Narasimhan,[a] J.W. Thybaut,[a] G.B. Marin,[a,*] Pierre A. Jacobs,[b] J.A. Martens,[b] J.F. Denayer,[c] and Gino V. Baron[c]

[a] *Laboratorium voor Petrochemische Techniek, Universiteit Gent, Krijgslaan 281, B-9000 Gent, Belgium*
[b] *Centrum voor Oppervlaktechemie en Katalyse, Katholieke Universiteit Leuven, Kasteelpark Arenberg 23, B-3001 Heverlee, Belgium*
[c] *Vrije Universiteit Brussel, Pleinlaan 2, B-1050 Brussel, Belgium*

Received 20 March 2003; revised 11 June 2003; accepted 19 June 2003

Abstract

A microkinetic model based on the single-event theory was developed to describe the hydroconversion of *n*-octane on Pt-H-ZSM-22 zeolite. In the model, alkene protonation and subsequent acid-catalyzed reactions, i.e., skeletal isomerization and cracking, occur in the pore mouths of ZSM-22. In contrast to USY, in these pore mouths, the molecules are physisorbed according to different modes, each with a specific enthalpy and entropy loss. Moreover after protonation of the physisorbed alkenes, the stability of the resulting carbenium ions increases with the number of carbon atoms entering the pore mouth. The reaction network is based on transformations of alkylcarbenium ions that can be obtained by protonation of physisorbed alkenes in pore mouths. Reactions that are sterically hindered or that lead to alkylcarbenium ions with charged carbon atoms outside the pore were discarded. In particular, methyl shifts as well as branching and β-scission reactions involving tertiary alkylcarbenium ions were excluded. The composite activation energy, $\Delta E_{\mathrm{act}}^{\mathrm{comp}}$, i.e., the sum of the protonation enthalpy and the real activation energy for the allowed reactions, was taken from data on a reference ultrastable Y zeolite (CBV760). This pore mouth catalysis model adequately describes the conversion of *n*-octane on Pt-H-ZSM-22. The difference in composite activation energy $\Delta E_{\mathrm{act}}^{\mathrm{comp}}$ of -8.9 (± 0.3) kJ mol^{-1} between the reference USY zeolite and the ZSM-22 corresponds to the higher average acid strength in ZSM-22. Further, the yield pattern of individual isomers of octane is described well using three parameters: (i) h_{cd} with a value of -1.1 (± 0.2) kJ mol^{-1} accounting for differences in carbenium ion stability proportional to the number of carbon atoms entering the pore mouth; (ii) ΔE_{pcp}; and (iii) ΔE_{β} with values of -4.0 (± 0.2) and -16.7 (± 2.1) kJ mol^{-1}.

Keywords: Single-event microkinetics; Hydrocracking; Hydroisomerisation; ZSM-22 zeolite; Shape selectivity; Kinetic modeling; *n*-Octane; Pore mouth catalysis

1. Introduction

Catalysts based on medium pore size zeolites such as ZSM-22 (TON-type), ZSM-5 (MFI-type), ZSM-11 (MEL-type), ZSM-23 (MTT-type), and AIPO-11 (AEL-type) allow petroleum refiners to meet the stringent quality requirements of fuels and lubricants. These zeolites display selectivity in hydrocarbon conversions [1,2] and, hence, play a key role in gasoline octane boosting, production of diesel with high cetane number and low pour point, and lubricating oil base stocks with high viscosity index (VI) and low pour point [3–8]. In the majority of these processes, the catalyst is bifunctional. Improving our understanding of reaction mechanisms in the confined environments of these medium pore size zeolites is essential to enable further catalyst and process optimization.

The conversion of hydrocarbon molecules on bifunctional zeolite catalysts follows a series of steps starting with transport of reactants from the bulk phase to the external catalyst pellet surface. The reactants diffuse inside the pellet macropores toward the individual zeolite crystals. This macropore diffusion is governed by molecular or Knudsen diffusion and does not contribute to selectivity for the kinetically controlled hydroconversion reactions described in the present paper. Further, the reactant alkanes physisorb into the micropores of the crystal lattice. Subsequently the reactant alkanes migrate to the metal sites where (de)-hydrogenation reactions take place. The alkenes formed on the metal sites mi-

* Corresponding author.
E-mail address: Guy.Marin@ugent.be (G.B. Marin).

0021-9517/$ – see front matter
doi:10.1016/S0021-9517(03)00281-1

grate back to the micropores of the crystal lattice where protonation occurs on the acid sites. Subsequently, the carbon skeleton is changed by isomerization or cracking. The selectivity of the catalytic conversion is strongly influenced by the shape and dimensions of the zeolite micropores [1,2]. The shape selectivity exhibited by zeolites can be classified as (i) reactant shape selectivity, (ii) product shape selectivity, and (iii) transition state shape selectivity [7,9] depending upon whether reactant diffusion, product diffusion, or the transition state is a limiting step. Besides these classic shape selectivity mechanisms inside the zeolite micropores, pore mouth catalysis is a special type of transition state shape selectivity involving adsorption and catalysis in the pore openings only.

The 10-membered rings of ZSM-22 have free diameters of 0.55×0.44 nm [10–12]. The channels are unidimensional and have undulations [12] with a repeat distance of ca. 0.5 nm. Unlike zeolites with wider pores such as ultrastable Y (US-Y), hydroconversion of long alkanes on ZSM-22-based catalysts results in high isomerization yields even at high conversion ($> 70\%$). For short alkanes up to decane, monobranched isomers with the methyl branch away from the central carbon atom are favored [11–16,19–26]. For undecane and longer alkanes there is a bimodal distribution of single methyl positions along the main chain [13,14]. The first maximum is at the C_2 position. The second maximum is broad and spans the methyl positions towards the center of the main chain starting from the C_5 position [14].

In order to explain the peculiar selectivity of ZSM-22 catalysts, pore mouth and key-lock mechanisms have been proposed based on circumstantial evidence [11–16,21–24]. In the pore mouth mechanism, a molecule is physisorbed in one pore mouth in such a way that one straight alkyl chain is inside the pore. The rest of the molecule remains outside [27]. The straight chain is either part of the main alkyl chain or else an *n*-alkyl substituent of the latter. A tertiary carbon atom carrying an *n*-alkyl branching is always outside the pore. Long molecules can span the distance between two or more pore openings on the external surface of the ZSM-22 zeolite crystal. These interactions are referred to as key-lock configurations.

Evidence for pore mouth mechanisms on ZSM-22 originates from experimental determinations of adsorption enthalpy and entropy of model molecules [25,28–31]. Those experiments showed that iso-alkanes do not enter the micropores, while *n*-alkanes do. In comparison to *n*-alkanes, Henry coefficients for iso-alkanes are one order of magnitude lower and the saturation capacity is three orders of magnitude lower resulting in very high separation factors between *n*-alkanes and iso-alkanes. The separation factors between normal and iso-alkanes are 4–5 times higher on ZSM-22 than on ZSM-5 or beta zeolites which have comparable and low separation factors despite the differences in pore dimensions. The distinctive high separation factors observed on ZSM-22 indicate that the pore dimensions are in between the size of normal and iso-alkanes. Physisorption experiments were performed by Ocakoglu et al. [31] on ZSM-22 samples with the organic template from the synthesis left inside, denoted as "closed" sample, and calcined ZSM-22 samples denoted as "open" sample. Iso-alkane physisorption enthalpies and entropies were observed to be the same on open and closed ZSM-22 [31]. This observation is strong evidence for the occurrence of pore mouth physisorption on ZSM-22. The dependency of the physisorption enthalpy on the methyl position in methylalkanes revealed that these branched molecules enter the pore until the branching hits the first 10 ring. The branching, along with the carbon atom carrying it, and the remainder of the main chain are left outside the pore. The above observations for alkanes are extendable to alkenes.

According to pore mouth catalysis, acid-catalyzed reactions occur at the pore mouths only. In the ideal situation, there is no molecular transport limitation from metal sites to acid sites [32]. Platinum, responsible for (de)-hydrogenation reactions, exists mostly on the external surface of the crystals as particles with diameters of ca. 3 nm, i.e., much larger than the channel diameters of ZSM-22 [19]. Park and Ihm [16] have even reported platinum particles with diameters as large as 23 nm in their catalytically active Pt-ZSM-22 preparation. Parton et al. [23] carried out experiments with mixtures of Pt-ZSM-22 and Pt-DB-Y (deep bed steamed Y-zeolite) and mixtures of Pt-ZSM-22 and DB-Y. It was found that the product distributions are similar in these zeolite mixtures with and without platinum on the Y zeolite, indicating fast intraparticle transport between metal and acid sites compared to chemical reaction steps. This shows that the tolerated distances for the intraparticle transport can be of the order of the diameters of the zeolite crystals, which is in the micrometer scale. On ZSM-22, the transport distances for the alkenes are short since the reactions occur at the pore mouths, and the platinum is on the external surface. While this is obvious for iso-alkenes, it also holds for *n*-alkenes. When *n*-alkenes penetrate entirely inside the pores and undergo branching, the resulting molecules are stuck in the channel. Therefore, effective *n*-alkene conversions occur in pore mouths only.

Maesen et al. [17,18] and Schenk et al. [34] published another interpretation of the selectivity patterns of ZSM-22. It was based on configurational bias Monte-Carlo (CBMC) calculations of physisorption equilibria in TON-type theoretical channels. In this approach, iso-alkane molecules are docked inside a pore model derived from crystallographic data and their mobility is estimated. Product diffusion selectivity was proposed to explain monomethyl branching, and transition state shape selectivity to explain dibranching. The authors assume not only the pore mouth acid sites, but also all acid sites inside the micropores to participate in the acid catalysis. This seems in contradiction with the recent experimental physisorption observations indicating steric hindrance for entry of iso-alkanes into the micropores. A very short time scale for diffusion from acid sites to metal sites is proposed allowing the assumption that the classical bifunctional mechanism [32] and the corresponding prod-

uct distribution are established inside the micropores. The observed product selectivities are attributed to differences in product diffusivities based on estimated apparent activation energies [17]. Nevertheless, these authors conclude that no diffusion limitations occur inside the ZSM-22 micropores. The absence of diffusion limitations is in contradiction with their explanation of product selectivities. Differences in product selectivities for the kinetically controlled process on ZSM-22 can only be explained by differences in kinetic steps at the pore mouth acid sites.

On Pt/ZSM-22 catalysts the reaction products have the features typical of ideal bifunctional catalysis [32,33]. The isomerization yields are high, monobranched and multibranched isomers are formed in consecutive reactions, there is limited cracking, and there is little methane and ethane formed. Such a situation is possible only if diffusion inside the micropores is not involved. Invoking transition state shape selectivity [35–37] to explain the hydroconversion on ZSM-22 also leads to the same inconsistency, as it necessitates diffusion of the molecules such that they are entirely inside the pores to enable the discrimination. For these reasons, the pore mouth catalysis model considering steric hindrance for full entry of branched molecules inside the pore mouths was adopted in the present kinetic modeling work of *n*-octane hydroconversion on Pt-ZSM-22.

Several modeling approaches including, e.g., discrete lumping [38,39], structure oriented lumping [40,41], continuum lumping [42,43], and single-event kinetics [44–46], have been developed to describe the complex reaction networks of hydrocracking and hydroisomerization. Of all the above approaches the single-event kinetics approach was selected in the present work because of its fundamental nature and capability to describe reaction networks involving alkylcarbenium ion chemistry in detail.

Hydroconversion of alkanes on USY has been modeled earlier using single-event kinetics [47,48] wherein the sum of protonation enthalpy and the real activation energy denoted as "composite activation energy" has been estimated for all the reaction families. These parameter values are linked to catalyst properties such as average acid site strength and have been found to be valid for a wide range of hydrocarbons on similar types of catalysts and is discussed in detail by Thybaut et al. [47]. The same set of parameters has been retained in the present work as reference in order to estimate the differences on ZSM-22.

2. Procedures

2.1. Catalyst

Preparation and characteristics of Pt-H-ZSM-22 catalysts were described by Ernst et al. [20]. The Si/Al ratio is 30. The elongated crystals measure from 1 to 2 μm. The platinum loading was 0.5 wt% and the average platinum particle size was 3 nm [13,19].

Table 1
Process conditions for experimental data on vapor-phase hydroconversion of *n*-octane on Pt-H-ZSM-22 [12,19,24]

Parameter	Range
W/F_0 (kg s mol^{-1})	14–460
Reaction temperature (K)	506
Pressure (bar)	4.5
H_2/HC ratio (molar)	13.13

2.2. Hydroconversion data

Experimental data on vapor-phase hydroconversion of *n*-octane were obtained in a tubular packed-bed reactor under the conditions reported in Table 1 [14,19]. Under these conditions "ideal" hydrocracking occurs; i.e., hydrogenation-dehydrogenation reactions are in quasi-equilibrium. Methane and ethane formation is negligible, indicative of the absence of hydrogenolysis activity. The selectivity for monobranched octane isomers decreased in the order: 2-methyl > 3-methyl > 4-methylheptane [19]. Dimethyl branching occurred to a negligible extent. The predominant dimethyl-branched molecule is 2,5-dimethylhexane [19] with a yield of only 3 mol% at a total *n*-octane conversion of 80 mol%. The contribution of key-lock catalysis is evident from the formation of 2,5-dimethylhexane, but is too small to obtain significant parameters related to key-lock catalysis. Hence key-lock catalysis is not included in this paper.

2.3. Reactor model and parameter estimation

The tubular packed-bed reactor was modeled based on a pseudo-homogeneous one-dimensional reactor model. The reactor was assumed to be fully isothermal and without any pressure drop. This leads to the following expressions for axial flow profiles through the reactor [49] for all alkanes of the reaction mixture except one (being the feed):

$$\frac{\mathrm{d}F_{P_j}}{\mathrm{d}W} = R_{P_j}. \tag{2.1}$$

The axial profile of the remaining *n*-octane was obtained from the atomic carbon balance. Hydrogen flow rates along the bed axis were calculated from the hydrogen atomic balance. The set of ordinary differential equations (ODEs) for axial flow profiles were integrated using the LSODA subroutine available on Net-Lib [50,51].

As the prominent reaction products are the individual monobranched isomers and the cracked products, they have been considered as responses for parameter estimation. Parameter estimations were performed using the nonlinear least-squares technique applying the Levenberg–Marquardt method for minimization of the objective function [52], i.e., the weighed sum of squared residuals from observed and calculated flow rates:

$$\mathrm{SSQ} = \sum_{j=1}^{\mathrm{nresp}} \sum_{k=1}^{\mathrm{nob}} w_{p_j} \left(F_{p_j,k} - \widehat{F}_{p_i,k}\right)^2. \tag{2.2}$$

ODRPACK-package version 2.01 [50,53] was used for regression. The calculation of weighing factors w_{p_j} was performed as described below [47]:

$$w_{p_j} = \frac{(\sum_{k=1}^{\text{nob}} F_{p_j,k})^{-1}}{\sum_{j=1}^{\text{nresp}} (\sum_{k=1}^{\text{nob}} F_{p_j,k})^{-1}}. \tag{2.3}$$

The outlet flow rates were calculated according to model equations described by Eq. (2.1) in conjunction with the expressions for the rate equations derived in the subsequent sections.

2.4. Single-event kinetic model of alkane conversion over Pt-H-USY zeolites

Hydroconversion reaction mechanisms occurring on Pt-H-zeolites were discussed in detail by Baltanas et al. [44] and Martens et al. [46]. Among the reactions occurring, the rate-determining steps are those involving C–C bond rearrangements, i.e., alkyl shifts, PCP branching reactions, and β-scissions [46]. As the oligomerization and hydride transfer reactions are found to be slow compared to the above reactions, they were excluded [47]. Protonation–deprotonation of alkylcarbenium ions and hydride shifts in alkylcarbenium ions were considered to be in quasi-equilibrium [44,46,47].

2.4.1. Rate-determining step

The reaction rate of the rate-determining steps was expressed as first order in the alkylcarbenium ion concentration [44]:

$$r_{\text{as/pcp/}\beta}(m_1, m_2) = k_{\text{as/pcp/}\beta}(m_1, m_2) C_{R_{i,k}^+}. \tag{2.4}$$

Using the single-event concept [44] symmetry effects are separated from the rate coefficient as follows,

$$k_{\text{as/pcp/}\beta}(m_1, m_2) = \frac{\sigma_{R_{i,k}^+}}{\sigma_{\neq}} \tilde{k}_{\text{as/pcp/}\beta}(m_1, m_2), \tag{2.5}$$

where $\sigma_{R_{i,k}^+}$ and $\sigma_{\neq}$ are global symmetry numbers of the reactants and the transition state. The ratio of the latter equals the number of single events corresponding to a given reaction step. The obtained single-event rate coefficients $\tilde{k}_{\text{as/pcp/}\beta}(m_1, m_2)$ depend only on the reaction family and the type of alkylcarbenium ions involved [46–48,54].

2.4.2. Rate equations

The alkylcarbenium ion concentration can be obtained from the physisorbed alkene concentration via a Langmuir relationship assuming that all acid sites are accessible for protonation of physisorbed alkenes. Considering that the total carbenium ion concentration on the acid sites is quite low [47] and accounting for the symmetry contribution for the (de)-protonation equilibrium coefficient, the alkylcarbenium ion concentration can be expressed as

$$C_{R_{i,k}^+} = C_t \frac{\sigma_{O_{i,j}}}{\sigma_{R_{i,k}^+}} \widetilde{K}_{\text{isom}}(O_{i,j}; O_r) \widetilde{K}_{\text{prot}}^{\text{usy}}(O_r; m_l) C_{O_{i,j}}, \tag{2.6}$$

where $\widetilde{K}_{\text{isom}}(O_{i,j}, O_r)$ is the single-event isomerization equilibrium coefficient between the alkene $O_{i,j}$ and the reference alkene O_r [45] calculated from thermodynamic data [55]. $\widetilde{K}_{\text{prot}}(O_r, m_l)$ is the single-event equilibrium coefficient for protonation of reference alkene to carbenium ion of type m_l, i.e., secondary or tertiary. As alkenes are assumed to have physisorption properties similar to that of alkanes [44,48,54], the alkene concentration in the above expression is related to physisorbed alkane concentration via the (de)-hydrogenation equilibrium relationship [44].

Multicomponent physisorption is described by an extended Langmuir isotherm. The concentration of physisorbed alkanes is related to gas-phase alkane partial pressure via the following Langmuir expression for physisorption:

$$C_{p_j} = \frac{K_{\text{L},i} C_j^{\text{sat}} p_i}{1 + \sum_{j=1}^{N} K_{\text{L},i} p_i}. \tag{2.7}$$

In this expression, the terms for physisorbed alkenes were omitted, considering that at quasi-equilibrium, the concentration of the latter is very low compared to that of the alkanes. The following rate expression for the elementary steps in terms of gas-phase alkane concentrations was obtained [47,54]:

$$\begin{aligned} &r_{\text{as/pcp/}\beta}(m_1, m_2) \\ &\quad = \frac{\sigma_{O_{i,j}}}{\sigma_{\neq}} \tilde{k}_{\text{as/pcp/}\beta}(m_1, m_2) \widetilde{K}_{\text{prot}}^{\text{usy}}(O_r, m_1) \widetilde{K}_{\text{isom}}(O_{i,j}; O_r) \\ &\qquad \times K_{\text{deh}} C_i^{\text{sat}} C_t K_{\text{L},i} p_i \Big/ \left(\left(1 + \sum_i K_{\text{L},i} p_i \right) p_{H_2} \right). \end{aligned} \tag{2.8}$$

In the above expression, K_{deh} is the equilibrium coefficient for (de)-hydrogenation, calculated using Benson's group contribution method [55]. The Langmuir physisorption coefficient, $K_{\text{L},i}$, for an alkane on a zeolite can be determined from its Henry coefficient and saturation concentrations as

$$K_{\text{L},i} = H_i / C_i^{\text{sat}}. \tag{2.9}$$

The net rate of formation of alkylcarbenium ion k originating from alkane i is obtained from the balance between its rate of formation and rate of disappearance:

$$\begin{aligned} R_{R_{i,k}^+} = &\sum_l \sum_o r_{\text{as/pcp}}(m_{l,o}; m_{i,k}) \\ &+ \sum_l \sum_o r_\beta(m_{l,o}; m_{i,k}, O_{u,v}) \\ &- \sum_l \sum_o r_\beta(m_{i,k}; m_{l,o}, O_{u,v}) \\ &- \sum_l \sum_o r_{\text{as/pcp}}(m_{i,k}; m_{l,o}). \end{aligned} \tag{2.10}$$

The net rate of formation of alkenes j corresponding to alkane i directly produced by β-scission is written as

$$R_{O_{i,j}} = \sum_l \sum_o r_\beta(m_{l,o}; m_{q,r}, O_{i,j}). \tag{2.11}$$

The net rate of formation of alkane i is the sum of all net rates of formation of the corresponding alkylcarbenium ions and of the net rate of formation of alkenes with the same skeletal structure formed via β-scissions:

$$R_{P_i} = \sum_{k=1}^{\mathrm{ncar}_i} R_{R_{i,k}^+} + \sum_{j=1}^{\mathrm{nole}_{i,\beta}} R_{O_{i,j}}. \tag{2.12}$$

The only parameters to be estimated in Eq. (2.8) by regression are the single-event rate coefficient and the single-event protonation–deprotonation coefficient. Due to low carbenium ion concentrations only the product of the two can be estimated. Hence, the composite rate coefficient is expressed as

$$\tilde{k}^{\mathrm{comp}}(m_1, m_2) = \tilde{K}^{\mathrm{usy}}_{\mathrm{prot}}(O_r, m_1)\tilde{k}(m_1, m_2). \tag{2.13}$$

The corresponding composite activation energy represents the sum of standard protonation enthalpy and the real activation energy of the rate-determining step:

$$E^{\mathrm{comp}}_{\mathrm{act}} = \Delta H^{\circ}_{\mathrm{prot}} + E_{\mathrm{act}}. \tag{2.14}$$

The values of the corresponding composite preexponential factors were calculated based on transition state theory [46]. Hence, only the composite activation energies for the rate determining reactions, i.e., alkyl shifts, PCP branchings, and β-scissions had to be estimated. This was previously done by regression of data obtained on Pt-H-USY zeolite (CBV760) [46,48,54,56].

Thybaut et al. [47] used a single adjustable parameter to account for activity differences among USY zeolites arising from differences in the average acid site strength. The model for one US-Y zeolite was applied to another one by adapting the standard protonation enthalpy of the involved alkenes, the latter being a measure of the average acid strength.

3. Physisorption of alkanes and alkenes on ZSM-22

In order to describe the hydroconversion kinetics on Pt/H-ZSM-22, it is essential to model accurately the physisorption of alkanes and alkenes in ZSM-22 pore mouths. Alkanes arriving from the bulk gas phase physisorb first on a pore mouth. n-Alkanes are subsequently transferred into the micropore connected with the pore mouth, while iso-alkanes remain at the pore mouth [27]. The transfer of n-alkanes from pore mouths into the micropores leads to significant additional entropy and enthalpy loss. The energy differences between pore mouth and crystal interior were previously experimentally determined using closed and open samples of ZSM-22, referred to in the Introduction [27,31]. A physisorption model distinguishing between physisorption at the pore mouth from physisorption into the micropores was developed in earlier work [27] and implemented here. At the pore mouths, n-alkanes physisorb fully into the pore mouth. In the case of iso-alkanes only one of its "straight ends" enter the pore mouth. The rest of the molecule is outside the pore mouth. This leads to different modes of physisorption for an alkane on a ZSM-22 pore mouth, depending on which straight end of the molecule is located inside the pore mouth and which moiety remains outside [27]. For example, 4-methyloctane has three physisorption modes pertaining to three straight ends viz. Fig. 1.

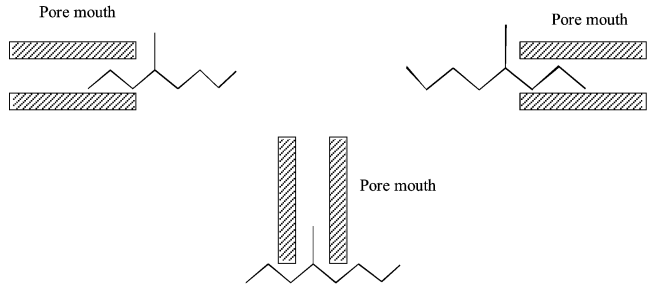

Fig. 1. Schematic representation of the three possible physisorption modes of 4-methyl octane at a ZSM-22 pore mouth indicated by parallel rectangular blocks.

Physisorption at pore mouths can be modeled by considering additivity of interactions of carbon atoms inside and outside the pore mouth with the crystal lattice in each of the physisorption modes. Due to stronger force fields inside the pore mouth the carbon atoms inside have higher energetic interactions compared to carbon atoms outside. These interactions contribute to standard enthalpy and entropy of physisorption, which are calculated by additivity [27]. Each physisorption mode has an equilibrium coefficient for physisorption on the pore mouths and denoted as $K_{i_m,\mathrm{pm}}$. The Langmuir isotherm expression can be used to describe the physisorption at pore mouths of ZSM-22 [27]. $K_{i_m,\mathrm{pm}}$ is estimated from standard physisorption enthalpy and entropy of individual physisorption modes. As in the case of H-USY, it is also expected that alkenes have identical physisorption properties as that of alkanes of similar skeletal structure on H-ZSM-22 [44,46,48,54]. Hence, in the development of the present model, physisorption of alkenes has been assumed identical to physisorption of alkanes.

4. Single-event kinetic model for hydrocracking and hydroisomerization on Pt-H-ZSM-22

4.1. Alkylcarbenium ion formation

Alkenes formed during dehydrogenation reactions on the metal sites migrate to the acid sites of the pore mouths where they are protonated. The steps involved in formation of an alkylcarbenium ion are illustrated in Fig. 2. (De)-protonation reactions occur much faster than the rate-determining acid-catalyzed isomerization and cracking and are assumed to be quasi-equilibrated [44,46,47,56]. Protonation for both branched and linear alkenes occurs at the pore mouths. Linear akylcarbenium ions can also exist inside the ZSM-22

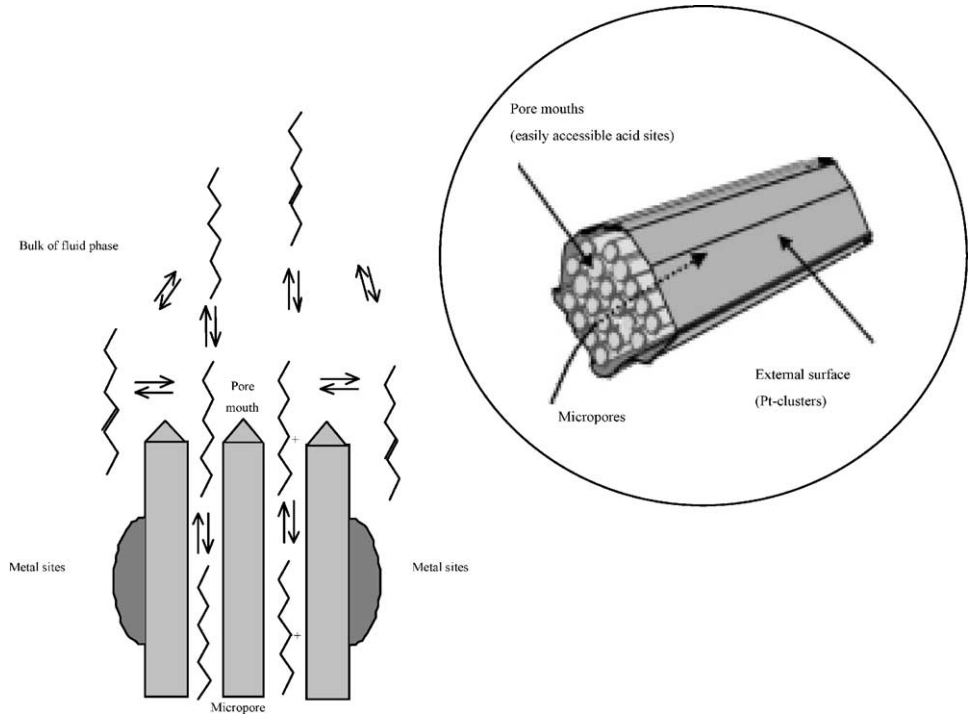

Fig. 2. Schematic representation of the elementary steps involved in carbenium ion formation on Pt-H-ZSM-22. Location of pore mouths, micropores, and metal sites on a ZSM-22 crystal are shown in the insert.

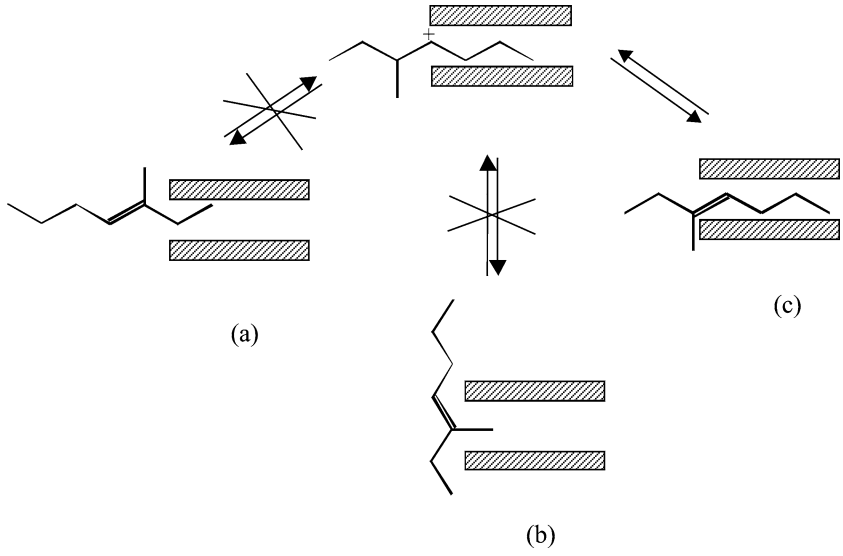

Fig. 3. Protonation possibilities of 3 methyl-hept-3-ene on a ZSM-22 pore mouth.

micropores. However, due to steric hindrance the branched alkylcarbenium ions are located only at the pore mouths. As the skeletal isomerization and cracking reactions always involve a branched alkylcarbenium ion either as a reactant or as a product, the productive alkyl carbenium ions are always located at the pore mouth. The carbenium ion formation depends on the mode of physisorption of the alkene in the physisorption step vide Fig. 3. It can be seen from Fig. 3, that protonation of an alkene can occur only in specific situations corresponding to (c) while for mode (a) and (b), protonation is impeded as the double bond is far away from the acid site at the pore mouth. Hence, every protonation corresponds to a specific physisorption mode, the energy of which can be calculated as explained in the preceding section [27]. This is the principal difference with USY zeolite, where physisorbed molecules can access any Brønsted acid site and be protonated. On ZSM-22, the acid site located in the pore mouth where the molecule is physisorbing is available only for that molecule for catalysis. Hence, the protonating chemisorption depends only on the number of Brønsted acid sites that

are located at the pore mouth and the probability of finding them empty. The Si/Al ratio of ZSM-22 is 30. The composition is homogeneous, as derived from XPS and bulk chemical analysis. Consequently, every three 10 rings, an Al atom and a corresponding acid site can be expected. Because the undulations along the ZSM-22 micropore are built from three 10 rings there is an acid site in each undulation [13,14]. Consequently, for a physisorbed alkene at the pore mouth, there is exactly one acid site within reach [13,14]. This acid site is unoccupied, as there is no space for a second molecule. Accordingly the carbenium ion concentration on ZSM-22 is described by

$$C_{R^+_{i_m,k}} = \frac{\sigma_{O_{i,j}}}{\sigma_{R^+_{i_m,k}}} \widetilde{K}_{\text{isom}}(O_{i,j}; O_r) \widetilde{K}^{\text{zsm-22}}_{\text{prot}}(O_r; m_l) C_{O_{i_m,j_k}}, \tag{4.1}$$

where $C_{O_{i_m,j_k}}$ is the concentration of alkene j belonging to alkane i of mode m resulting in carbenium ion k belonging to the same mode m. Note that the units of the protonation equilibrium coefficient on ZSM-22, $\widetilde{K}^{\text{zsm-22}}_{\text{prot}}(O_r; m_l)$ correspond to that of $C_t \widetilde{K}^{\text{usy}}_{\text{prot}}(O_r; m_l)$. The quantity corresponding to C_t on ZSM-22 equals the product of the number of acid sites located at the pore mouth and the probability of finding them empty which equals one and, therefore, is not explicitly noted. On ZSM-22, only the physisorption at the pore mouths is competitive and the protonating chemisorption for the physisorbed alkene at the pore mouth is noncompetitive. This is in contrast to USY where both physisorption and chemisorption are competitive. The ratio of acid sites to physisorption concentration upon saturation on USY viz. Table 3 is approximately a factor of 3 lower than that of ZSM-22 where the ratio equals unity. The preexponential factor of the protonation equilibrium coefficient is calculated by extension of the methodology followed while modeling the kinetics on USY [46]. This is described further in Section 4.5. As described in Section 2.4.2, the protonation enthalpy is contained in the composite activation energy which is estimated through regression. The protonation enthalpy depends on the acid site strength. While it is independent of carbon number for higher alkanes on USY, it has a carbon number dependency for molecules with carbon numbers up to nine due to charge delocalization effects [47], such as the inductive effect and hyperconjugation. The concept is assumed to be extendable to ZSM-22. On ZSM-22, the delocalized charge on the carbon atoms inside the pore mouth interacts strongly with the deprotonated acid site and contributes to the carbenium ion stability. A linear relationship is proposed between the charge delocalization effect and the number of carbon atoms entering the pore mouth.

4.2. Alkylcarbenium ion reactions

In a USY zeolite, the micropores are freely accessible to alkane and alkene molecules. There is no discrimination between physisorption modes. As a result, protonating chemisorption and the full network of subsequent acid-catalyzed reactions based on free carbenium ion chemistry is possible. In contrast to USY, on ZSM-22 only acid-catalyzed reactions pertaining to a given physisorption mode can occur in a pore mouth mechanism. Reactions that necessitate a change of physisorption mode of the alkylcarbenium ion, whereby the ionic center of the molecule has to leave the confined space of the poremouth, are considered unlikely and are discarded from the model. Other reactions involving, e.g., the formation of tertiary carbon atoms inside the pore are sterically suppressed on ZSM-22. As a starting point, a reaction network generation algorithm [45] generating all possible reactions, reactants, products, and intermediates based on alkylcarbenium ion chemistry was used [46]. Subsequently, this reaction network was limited to reactions that are allowed in a pore mouth mechanism on ZSM-22. This adaptation requires consideration of physisorption modes, protonating chemisorption, and steric effects. All together, it resulted in the formulation of a set of rules for pore mouth catalysis.

4.2.1. Formation of tertiary alkylcarbenium ions is sterically suppressed

Tertiary carbenium ions are formed due to protonation of an alkene which has a tertiary carbon atom involved in the carbon–carbon double bond. On ZSM-22, the carbon atom carrying the branch is outside the pore mouth and hence too far from the acid site to lead to a stable carbenium ion:

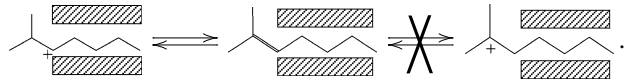

This rule follows from the suggestions of Souverijns et al. [12] to describe the high isomerization along with low cracking yield and peculiar isomer yield pattern on ZSM-22 in contrast to USY. For example, the occurrence of tertiary carbenium ion is expected to result in a preferential formation of 2,2-dimethyl-branched isomers and high cracking rates. As low cracking rates and no significant amounts of geminally dibranched isomers are observed experimentally [12–14], the formation of tertiary carbenium ions is excluded on ZSM-22. Consequently, hydride shift reactions involving conversion of a secondary into a tertiary alkylcarbenium ion, or vice versa, a tertiary into a secondary alkylcarbenium ion are discarded. Such reactions require the ionic center of the molecule to leave the pore mouth:

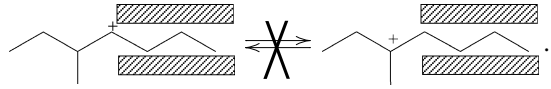

Tertiary alkylcarbenium ions occur in several β-scission reactions such as cracking of geminal dibranched molecules. Such reactions are also discarded:

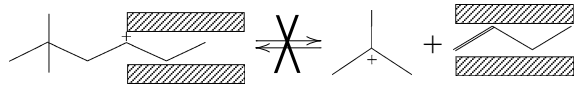

In summary, all alkylcarbenium ion transformation reactions in which either the original or the product ion, or

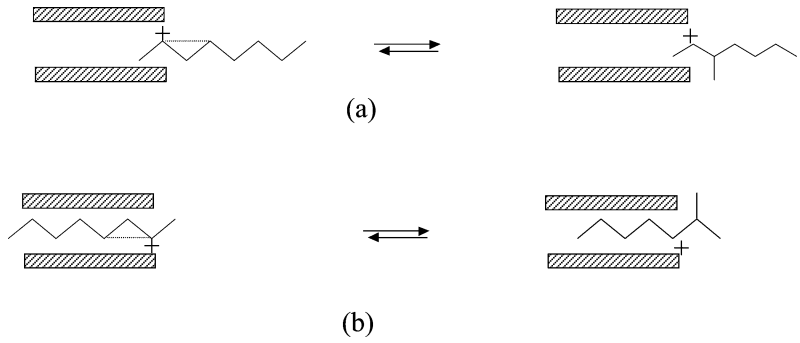

Fig. 4. Possible protonated states for 2-octyl carbenium ion.

both, is of a tertiary nature are considered to be entirely suppressed. The allowed reactions involve only secondary alkylcarbenium ions as described below.

4.2.2. Skeletal rearrangement of linear, secondary alkylcarbenium ions is allowed at all carbon positions

As described in the preceding section, protonation of linear alkenes occurs in the pore mouth. The positively charged carbon atom is always located inside the pore mouth. This gives rise to different possible configurations. For example, the 2-octyl carbenium ion has two protonated states viz. Fig. 4. In state (a) the number of carbon atoms inside the pore mouth is 2 while in state (b) it is 7. A PCP on a ZSM-22 pore mouth decomposes with the charge-bearing carbon atom inside the pore mouth. PCP branching of the alkylcarbenium ion in state (a) leads to 3-methylheptyl carbenium ion, while for state (b) the product is 2-methylheptyl carbenium ion. It is to be noted here that the alkylcarbenium ion in state (b) is formed from the alkene with the largest number of carbon atoms inside the pore mouth and, hence, is the most favored. State (a) is less favored because the physisorption is relatively less stable compared to state (b). As a result, 2-methylheptane is the most favored isomer on ZSM-22.

4.2.3. Rearrangement of branched secondary carbenium ions is allowed

Branched alkylcarbenium ions are formed through protonation of branched alkenes at pore mouths, depending on the physisorption mode. For example, protonation of 3-methylhept-3-ene, 3-methylhept-4-ene, and 3-methylhept-5-ene occurs in the same physisorption mode "A" on ZSM-22 with possible positions of the charge-bearing carbon atom as 4, 5, and 6, respectively:

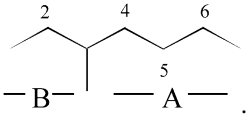

Protonation of 3-methylhept-2-ene occurs through a different physisorption mode "B." As the carbenium ion cannot leave the pore mouth, only rearrangements of secondary alkylcarbenium ions which do not alter the physisorption mode can occur. All other reactions requiring a change of physisorption mode with concomitant long separation of the negative framework charge from the positively charged carbon atom are unlikely in a pore mouth mechanism. The following examples illustrate such situations:

4.2.3.1. Alkyl shifts leading to shifts of branching positions are not allowed In the alkyl shift reactions, the alkyl group and the carbenium ion switch positions which leads to a shift in the branching positions on the main chain of the alkane. On ZSM-22 this requires the ionic center of the molecule to leave the pore mouth, which is considered to be unlikely:

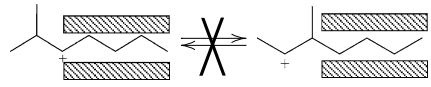

The exclusion of alkyl shifts at the pore mouth acid sites follows the same logic put forth for exclusion of tertiary carbenium ions [12]. The positional shift of the ionic center required for the formation of the product carbenium ion during the isomerization is even farther than that of the tertiary carbenium ion and hence cannot stabilize. This situation on ZSM-22 is remarkable. Alkyl shifts are known to be fast reactions on large pore zeolites.

4.2.3.2. PCP structures with quaternary carbon atom are not allowed Geminally dimethyl-branched isomers are observed experimentally only in negligible amounts [12–15,22]. Although the reactant carbenium ion is stable, it can be concluded that the charge in the corresponding activated complex which involves bonding with a tertiary carbon atom cannot be stabilized at the pore mouth due to steric hindrance. Hence, isomerization through PCP formation involving a secondary carbenium ion and a tertiary carbon atom at the β position of the positively charged carbon is sterically hindered and excluded.

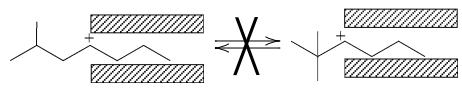

As a consequence of the above steric hindrance, isomerization leading to geminal dibranching reactions do not occur in a pore mouth mechanism on ZSM-22. Vicinal dibranching resulting from the above carbenium ion is also

suppressed. However, isomerization leading to vicinal dibranching can occur in a pore mouth mechanism on ZSM-22 via alternative PCP branching reactions.

4.2.3.3. Reactions involving an alkylcarbenium ion with a branch on either side of the charged carbon atom along the main chain are not allowed As the tertiary and quaternary carbon atoms cannot enter the pore mouth, alkenes with the double bond located in between two such carbon atoms cannot be protonated in pore mouths. Secondary–secondary PCP branching leading to a product carbenium ion with a branch on either side of the charged carbon atom is also inhibited as there exists no permitted protonation state for such carbenium ions in the pore mouths:

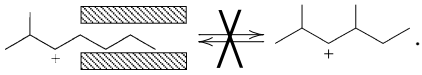

The exclusion of alkylcarbenium ions with a branch on either side of the charged carbon atom at the pore mouth acid sites also follows the same suggestion put forward for exclusion of tertiary carbenium ions [12], i.e., position of ionic center far from the acid site to stabilize. Although this rule is generally valid in pore mouth mode, for longer molecules such types of carbenium ions are possible in key-lock mode. This mode requires a minimum of three methylene groups between the two branches [13–15,24]. The contribution of key-lock catalysis to the observed product distribution is small when dealing with the relatively short *n*-octane molecule. A further consequence of the assumption is that secondary–secondary β-scission reactions of alkylcarbenium ions with the charged carbon atom located in between the two branchings are excluded:

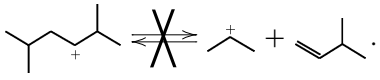

A comparison of reactions occurring in pore mouth catalysis on ZSM-22 vis-à-vis reactions occurring on USY is summarized in Table 2.

4.2.3.4. Changes of physisorption during the course of reaction In addition to the above rules, changes in physisorption occur during the course of reactions and have to be accounted for. During PCP branching, the location of the charge shifts from reactant state to transition state and further to product state. In all these cases, changes in physisorption enthalpy and entropy occur due to variations in numbers of carbon atoms inside and outside the pore. These variations in physisorption enthalpy and entropy can be calculated via the methodology discussed in Section 3 [27]. For PCP reactions leading to branching, the transition state moves outward from the pore mouth. This corresponds to late transition state:

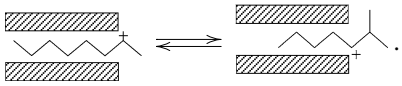

Table 2
A comparison of composite activation energies for acid-catalyzed reactions occurring on USY and ZSM-22 for hydroconversion reaction network based on free carbenium ion chemistry

Acid-catalyzed reactions (type)	$\Delta E_{act}^{comp\text{-}usy}$ (kJ mol^{-1})[a]	$\Delta E_{act}^{comp\text{-}zsm\text{-}22}$ (kJ mol^{-1})
Alkyl shift (s,s)	16.7	×
Alkyl shift (s,t)	13.7	×
Alkyl shift (t,s)	13.7	×
Alkyl shift (t,t)	7.7	×
PCP branching (s,s)	45.6	32.8–39.4[b]
PCP branching (s,t)	38.8	×
PCP branching (t,s)	38.8	×
PCP branching (t,t)	31.5	×
β-Scission (s,s)	79.2	53.7–60.3[b]
β-Scission (s,t)	63.7	×
β-Scission (t,s)	55.1	×
β-Scission (t,t)	33.9	×

All reactions of secondary and tertiary carbenium ions occur on USY while only some secondary–secondary reactions can occur via pore mouth mechanism on ZSM-22. ×, excluded; s, secondary; t, tertiary.

[a] Thybaut et al. [47].

[b] Estimated through regression. The range is due to variations in protonation enthalpy due to the number of carbon atoms entering the pore mouths.

Hence, the physisorption state of the transition state is considered to be the same as that of the product carbenium ion. In the above illustration it corresponds to an outward shift of two carbon atoms from the reactant state, i.e., the reactant carbenium ion has 7 carbon atoms inside the pore mouth and one carbon atom outside while the product carbenium ion has 5 carbon atoms inside and three carbon atoms outside. Upon physisorption the enthalpy loss per carbon atom inside the pore mouth is 12.8 kJ mol^{-1} and that of carbon atoms outside is 6.8 kJ mol^{-1} [27]. This results in a net enthalpy gain of 11.8 kJ mol^{-1} while going through the forward reaction. A similar calculation for entropy results in an entropy gain of 16 J mol^{-1} K^{-1}. The reverse reaction, i.e., debranching has an early transition state and no shift in physisorption state occurs during the transition state. β-scission reactions can be assumed to have an early transition state:

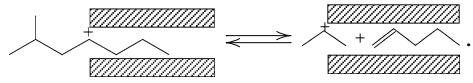

The transition state for forward reaction leading to cracking of the carbenium ion corresponds to the reactant carbenium ion state and no shift in the physisorption state is assumed.

4.3. Rate equations

As a result of the above rules, some secondary–secondary PCP and β-scission reactions need to be considered. The rate expression derived for alkane conversion on Pt/USY, viz. Eq. (2.8), is transformed into the following equation pertain-

ing to Pt/ZSM-22 catalyst:

$$r_{\mathrm{pcp}/\beta}(m_1, m_2) = \frac{\sigma_{O_{i,j}}}{\sigma_{\neq}} \tilde{k}_{\mathrm{pcp}/\beta}(m_1, m_2) \widetilde{K}_{\mathrm{prot}}^{\text{zsm-22}}(O_r, m_1) \widetilde{K}_{\mathrm{isom}}(O_{i,j}; O_r) \times \widetilde{K}_{\mathrm{deh}} C_{t,\mathrm{pm}} K_{i_{mm_2},\mathrm{pm}} p_i \Big/ \left(\left(1 + \sum_i \sum_m K_{i_m,\mathrm{pm}} p_i \right) p_{\mathrm{H}_2} \right). \quad (4.2)$$

The Langmuir physisorption coefficient in Eq. (2.8) refers to the physisorption state during reaction at pore mouths, viz., $K_{i_{mm_2},\mathrm{pm}}$. The C_i^{sat} in Eq. (2.8) corresponds to the number of pore mouths $C_{t,\mathrm{pm}}$ in Eq. (4.2) as the physisorption leading to reaction is limited to the pore mouths on ZSM-22. As discussed in Section 4.1, C_t in the case of ZSM-22 corresponds to unity.

4.4. Composite activation energies

The composite activation energy expressed in Eq. (2.14) for the PCP branchings and β-scission reactions on ZSM-22 is related to the corresponding composite activation energy on the reference USY zeolite CBV-760 [46] and is expressed as follows:

$$E_{\text{act-pcp}/\beta}^{\text{comp-ZSM-22}} = E_{\text{act-pcp}/\beta}^{\text{comp-USY}} + \Delta E_{\text{act-pcp}/\beta}^{\mathrm{comp}}, \quad (4.3)$$

where $\Delta E_{\text{act-pcp}/\beta}^{\mathrm{comp}}$ accounts for the differences in average acid site strength [47] between reference USY and ZSM-22 as well as for the possible differences in the actual activation energy of the rate-determining steps. Hence $\Delta E_{\text{act-pcp}/\beta}^{\mathrm{comp}}$ consists of two terms:

$$\Delta E_{\text{act-pcp}/\beta}^{\mathrm{comp}} = \Delta E_{\text{act-pcp}/\beta} + \Delta(\Delta H)^{\mathrm{prot}}, \quad (4.4)$$

where $\Delta E_{\text{act-pcp}/\beta}^{\mathrm{comp}}$ depends on the type of reactions involved in the rate-determining step and $\Delta(\Delta H)^{\mathrm{prot}}$. The latter term which is independent of the type of reaction is the difference in standard protonation enthalpy between reference USY and ZSM-22.

4.5. Preexponential factor

Preexponential factors were calculated based on transition state theory [46,48,54]. The preexponential factor of the composite rate coefficient is determined by the standard protonation entropy and the standard activation entropy. In the model for hydroconversion on Pt-H-USY zeolite it has been assumed that physisorption and protonation will ultimately result in the molecule losing its translational entropy [46,48,54]. On ZSM-22, the molecule is assumed to lose some amount of rotational freedom in addition to the translational entropy:

$$\Delta S_{\mathrm{prot}}^{\circ} + \Delta S_{\mathrm{phys}}^{\circ} = -S^{\mathrm{trans}} - S_{i,\mathrm{rot}}, \quad (4.5)$$

where S^{trans} is the translational entropy of the free molecule and $S_{i,\mathrm{rot}}$ is the sum of internal rotational entropy contributions. Among the isomers of octane the maximum degree of freedom lost is for the 2-methyl hept-3-yl carbenium ion as it has the longest straight end inside the pore mouth. The additional loss in rotational freedom for this molecule is assumed to be equivalent to the internal rotational entropy contribution of the three methylene groups and the methyl group of the straight end present inside the pore mouth. Hence, both terms on the right-hand side of Eq. (4.5) can be obtained from statistical thermodynamics. As the standard physisorption entropy, $\Delta S_{\mathrm{phys}}^{\circ}$ has been determined independently by Laxmi Narasimhan et al. [27] Eq. (4.5) allows calculation of the standard protonation entropy $\Delta S_{\mathrm{prot}}^{\circ}$. The total entropy loss upon physisorption and protonation for other carbenium ions is lower than that of the reference 2-methyl-hept-3-yl carbenium ion because of the lower number of carbon atoms inside the pore mouth and, hence, the lower number of degrees of free rotation which are hindered. The dependence of the right-hand side of Eq. (4.5) on the carbon atoms inside the pore mouth is entirely attributed to differences in $\Delta S_{\mathrm{phys}}^{\circ}$ on the left-hand side of the equation. As a result the standard protonation entropy, $\Delta S_{\mathrm{prot}}^{\circ}$, can be considered as constant, independent of the molecule considered. The above approximation is reasonable as appreciable differences in protonation entropy are not expected among the secondary carbenium ions. The transition state entropy accounts for the entropy difference between the reactant state and the transition state. Martens et al. [46,48,54,56] have estimated the transition state entropy for PCP and β-scission reactions on the USY where steric hindrance has a negligible effect. On ZSM-22, due to narrow pore structures steric hindrance can possibly have its influence on the transition state entropy. However, as a first approximation, the same transition state entropy as that assumed for the reference USY by Martens et al. [46,48,54,56] has been considered.

5. Composite activation energy differences between Pt-H-USY and Pt-H-ZSM-22

5.1. Reaction family independent

In the first instance, the validity of the assumptions on which the model is based was tested by regression of the experimental data with one adjustable parameter, $\Delta E_{\mathrm{act}}^{\mathrm{comp}}$, accounting for the differences in composite activation energy between ZSM-22 and USY. These differences were assumed to be reaction family independent. The estimated value of $\Delta E_{\mathrm{act}}^{\mathrm{comp}}$ amounted to -8.9 (± 0.3) kJ mol^{-1}. This results in higher turnover frequencies on ZSM-22 compared to the reference USY, viz. Fig. 5, and is attributed to a higher average acid site strength of ZSM-22. An F value of 2000 was obtained, corresponding to a global significance of regression. Physisorption and protonation properties of reference USY and ZSM-22 are compared in Table 3. The standard physisorption enthalpy on ZSM-22 is significantly higher than on USY. Strong physisorption contributes to higher reaction rates. As explained in Section 4.1 the acid site for

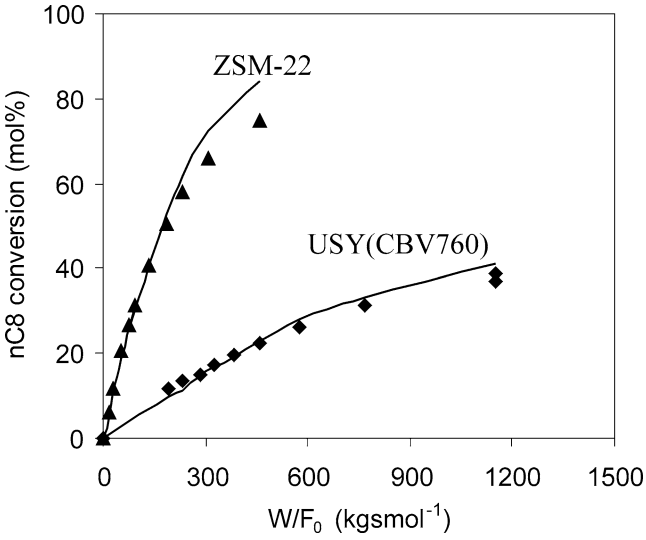

Fig. 5. Conversion of *n*-octane as a function of space time: experimental (symbols) and calculated (lines): (▲) on Pt-H-ZSM-22, obtained by regression of kinetic model with a single adjustable parameter: Eqs. (2.1)–(2.3) along with Eqs. (4.2)–(4.5) with experimental data described in Table 1, (◆) on Pt-H-USY(CBV 760) reported by Thybaut et al. [47].

Table 3
A comparison of physisorption and acidic characteristics of USY and ZSM-22

	Reference USY[a]	ZSM-22[b]
C_i^{sat} (mmol $\text{kg}_{\text{cat}}^{-1}$)	620	0.34[c]
C_t (mmol $\text{kg}_{\text{cat}}^{-1}$)	210	540[d]
$C_{t,\text{pm}}$ (mmol $\text{kg}_{\text{cat}}^{-1}$)	–	0.34
$\Delta H^{\circ}_{\text{phy}}$ for *n*-octane (kJ mol^{-1})	−55.9	−101.0

[a] Thybaut et al. [47].
[b] Ocakoglu et al. [31].
[c] For pore mouth physisorption saturation capacity equals the number of pore mouths.
[d] Total acid sites: out of this the acid sites on which reactions occur equals the number of pore mouths.

alkene protonation on ZSM-22 can only be accessed by the alkene physisorbed in the pore mouth where the acid site is located, unlike on USY, where all alkenes can access any acid site. This also contributes to higher specific reaction rates on ZSM-22.

An adequate description of conversion versus space time was obtained during regression as shown in Fig. 5. Isomerization is adequately described as can be seen from Fig. 6. Physisorption and subsequent fast hydride shift reactions determine the most abundant reactive intermediates (*MARI*) to be those with a maximum number of carbon atoms inside the pore mouth [27]. Accordingly among the carbenium ions of monobranched isomers of octane, the *MARIs* can be ranked as 2-methyl-hept-3-yl carbenium ion > 3-methyl-hept-4-yl carbenium ion > 4-methyl-hept-5-yl carbenium ion. The same ranking is observed in the product pattern of the corresponding isomers of octane. The selective formation of 2-methylheptane was described accurately, along with the preference of 3-methylheptane over 4-methylheptane formation viz. Fig. 7. This shows that the features of pore mouth catalysis are in first approximation taken into account in the model.

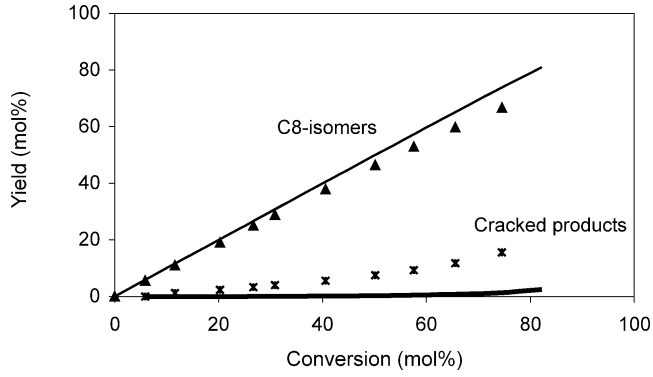

Fig. 6. Isomerization and cracking conversions of *n*-octane as a function of total conversion obtained by regression of kinetic model with a single adjustable parameter: Eqs. (2.1)–(2.3) along with Eqs. (4.2)–(4.5) with experimental data on C8 hydroconversion on Pt-H-ZSM-22 described in Table 1. Symbols: experimental, (▲) isomers; (∗) cracked products. Solid lines: calculations.

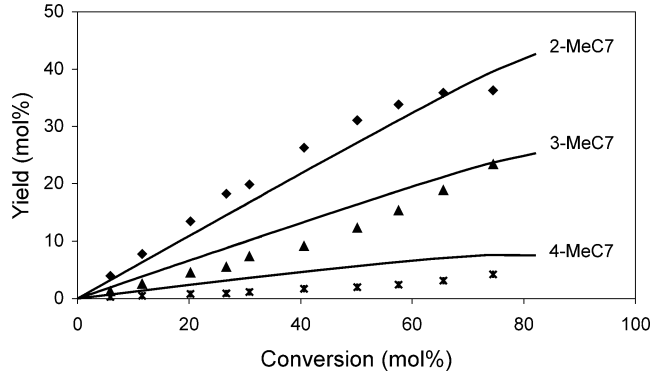

Fig. 7. Distribution of monobranched octane isomers: obtained by regression of kinetic model with a single adjustable parameter: Eqs. (2.1)–(2.3) along with Eqs. (4.2)–(4.5) with experimental data on C8 hydroconversion on Pt-H-ZSM-22 described in Table 1. Symbols: experimental, (◆) 2MeC7; (▲) 3MeC7; (∗) 4MeC7. Solid lines: calculations.

5.2. Reaction family dependent

Although the yield of total isomers is predicted reasonably, the cracking is underpredicted by the model vide Fig. 6. Also there are deviations from experimental data in the prediction of individual isomer yields vide Fig. 7. The deviations are due to assumed identical differences in composite activation energy for both isomerization and cracking reactions. The stability of secondary alkylcarbenium ions depends on inductive effects, and especially on the number of carbon–carbon bonds in β position to the positively charged carbon [47]. The estimated composite activation energy represents an average value for all these secondary alkylcarbenium ions. On ZSM-22, the reactions that are retained in the model involve secondary carbenium ions with least stabilization by inductive effect, because of the linear nature of the

alkyl chain. This results in a difference in composite activation energy compared to USY. For the same reasons of alkylcarbenium ion stabilities, there is also a difference in the activation energy of secondary–secondary PCP and β-scission reactions on secondary alkylcarbenium ions which needs to be accounted for.

In addition, the protonation enthalpy is dependent on the number of carbon atoms present inside the pore. Thybaut et al. [47] determined the dependency of protonation enthalpy on carbon number for alkanes in the range C5–C9 on the USY zeolite, i.e., a situation where all carbon atoms of the molecules enter the crystal pores. A strong dependency of protonation enthalpy on carbon number is also expected to occur on ZSM-22, especially since the number of carbon atoms inside the pore is limited. Considering the above, in the second term in the right-hand side of Eq. (4.4), $\Delta E^{\text{comp}}_{\text{act-pcp}/\beta}$ can be expressed as

$$\Delta E^{\text{comp}}_{\text{act-pcp}/\beta} = \Delta E_{\text{act-pcp}/\beta} + \Delta(\Delta H^{\circ}_{\text{prot-acidity}}) + \Delta(\Delta H^{\circ}_{\text{prot-CN}}), \tag{5.1}$$

where $\Delta E_{\text{act-pcp}/\beta}$ accounts for the changes in the activation energy for PCP and β-scission reactions, $\Delta(\Delta H^{\circ}_{\text{prot-acidity}})$ for acid site strength differences, and $\Delta(\Delta H^{\circ}_{\text{prot-CN}})$ for carbon number dependency of the protonation enthalpy. Based on the carbon number dependency observed on USY [47], a linear relationship for the dependency on the number of carbon atoms inside the pore mouth is assumed:

$$\Delta(\Delta H^{\circ}_{\text{prot-CN}}) = h_{\text{cd}} CNP. \tag{5.2}$$

Since $\Delta E_{\text{act-pcp}/\beta}$ and $\Delta(\Delta H^{\circ}_{\text{prot-acidity}})$ cannot be separately estimated, the combination of the two is estimated and represented as $\Delta E_{\text{pcp}/\beta}$:

$$\Delta E_{\text{pcp}/\beta} = \Delta E_{\text{act-pcp}/\beta} + \Delta(\Delta H^{\circ}_{\text{prot-acidity}}). \tag{5.3}$$

The above considerations lead to ΔE_{pcp}, ΔE_{β}, and h_{cd} as model parameters to be estimated from regression. An F value of 1600 was obtained. The regression results vide Table 4 confirm that ΔE_{pcp} and ΔE_{β} are different indeed. The ΔE_{pcp} was estimated less negative, i.e., -4.0 (± 1.1) kJ mol^{-1} than ΔE_{β}, i.e., -16.7 (± 2) kJ mol^{-1}. The parameter h_{cd} has been estimated to be -1.1 (± 0.2) kJ mol^{-1} per carbon atom inside the pore, which indicates interaction of the delocalized charge with the deprotonated acid site on ZSM-22 comparable to that reported for lower carbon number carbenium ions on USY [47]. The maximum binary correlation observed between h_{cd} and ΔE_{pcp} is 0.7. As a result of the above parameters the composite activation energies for PCP and β-scission reactions vary with carbenium ions due to differences in the number of carbon atoms inside the pore mouth. For PCP reactions the composite activation energy varies between 32.8 and 39.4 kJ mol^{-1} as compared to 45.6 kJ mol^{-1} for the reference USY, viz. Table 2, with the lowest corresponding to 2-methyl-hept-3-yl carbenium ion. This also contributes to formation of 2-methyl heptane as the most dominant product on ZSM-22. The number of carbon atoms inside the pore mouth contributes to the ranking of *MARIs* described in Section 5.1.

Table 4
Parameters estimated by regression of the kinetic model with three adjustable parameters: Eqs. (2.1)–(2.3) along with Eqs. (4.2)–(4.5) and (5.1)–(5.3) with experimental data on C8 hydroconversion on Pt-H-ZSM-22 described in Table 1

Parameter (kJ mol^{-1})	Value ($\pm$95% confidence limit)
ΔE_{pcp}	-4.0 (± 1.1)
ΔE_{β}	-16.7 (± 2.1)
h_{cd}	-1.1 (± 0.2)

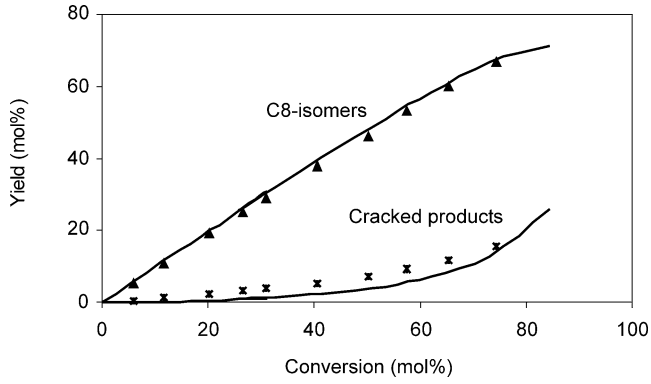

Fig. 8. Isomerization and cracking conversions of n-octane as a function of total conversion: obtained during regression of kinetic model with three adjustable parameters: Eqs. (2.1)–(2.3) along with Eqs. (4.2)–(4.5) and (5.1)–(5.3) with experimental data on C8 hydroconversion on Pt-H-ZSM-22 described in Table 1. Symbols: experimental, (▲) isomers; (∗) cracked products. Solid lines: calculations.

For β-scission reactions the composite activation energies vary between 53.7 and 60.3 kJ mol^{-1} compared to 79.2 kJ mol^{-1} for the reference USY viz. Table 2. These values imply that on a relative basis, there is more cracking on ZSM-22 compared to the USY case. At first sight, this seems contradictory to the experimental observation of higher isomer yields obtained on ZSM-22 compared to USY. The explanation is that the fastest cracking mechanism involving tertiary alkylcarbenium ions is entirely suppressed on ZSM-22, and this suppression of a fast cracking mechanism overcompensates the enhanced cracking via secondary–secondary β-scission. This is evident from the activation energy of tertiary–tertiary β-scission reactions on USY which is 40–45 kJ mol^{-1} lower than the activation energy of secondary–secondary β-scission reactions [47,56].

The model based on final regressed values of the parameters is better than the single parameter model discussed above. The description of conversion versus space time is similar to that shown in Fig. 5. Fig. 8 shows that the trends of isomerization and cracking are in excellent agreement with experimental data. Finally, Fig. 9 shows that the distributions of monobranched isomers are described better compared to the single parameter model.

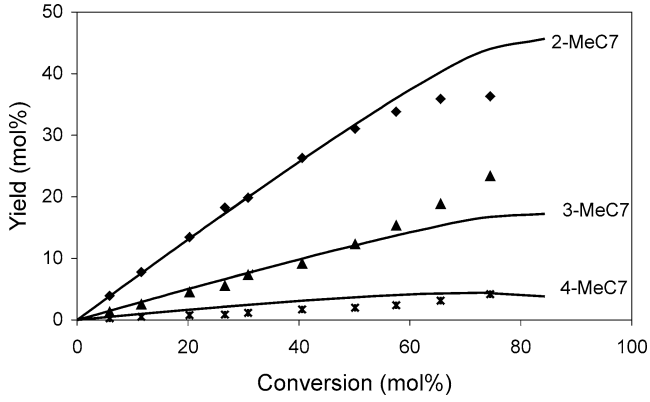

Fig. 9. Distribution of monobranched octane isomers: obtained during regression of kinetic model with three adjustable parameters: Eqs. (2.1)–(2.3) along with Eqs. (4.2)–(4.5) and (5.1)–(5.3) with experimental data on C8 hydroconversion on Pt-H-ZSM-22 described in Table 1. Symbols: experimental, (◆) 2MeC7; (▲) 3MeC7; (∗) 4MeC7. Solid lines: calculations.

6. Conclusions

The hydroconversion on Pt/H-ZSM-22 of a model alkane such as *n*-octane can be accurately described by a microkinetic model using the single-event methodology. Via a set of rules, pore mouth catalysis can be accounted for at the level of physisorption and protonation as well as the transition states.

Individual alkanes and alkenes can be physisorbed in a pore mouth according to different modes. These modes lead to formation of specific alkylcarbenium ions, the transformations of which are also subjected to severe limitations. The most significant limitation is that the tertiary alkylcarbenium ions do not occur on ZSM-22.

The higher reaction rates on ZSM-22 are mainly due to a higher average acid strength compared to USY. Physisorption at ZSM-22 pore mouths is competitive while the subsequent protonation of the physisorbed alkene is noncompetitive. This also contributes to higher specific reaction rates on ZSM-22 compared to USY where both physisorption and protonation are competitive.

One parameter representing a unique difference in composite activation energy suffices to account for the difference in conversion obtained on Pt/H-ZSM-22 with respect to Pt/H-USY. A more detailed model allowing reaction family-dependent differences in composite activation energies and a carbon number-dependent protonation enthalpy is required to adequately describe the selectivities observed on Pt/H-ZSM-22. The reaction family-dependent differences in composite activation energies arise from the exclusion from the model of specific PCP and β-scission reactions, occurring in USY but not in ZSM-22 pore mouths. The secondary alkylcarbenium ions involved in ZSM-22 catalysis represent the ions which are least stabilized by inductive effects. β-Scission involves secondary alkylcarbenium ions with on average a higher stability than those involved in PCP isomerization.

7. Nomenclature

7.1. Roman symbols

C	Concentration (mol kg_{cat}^{-1})
C_t	Total concentration of Brønsted acid sites (mol kg_{cat}^{-1})
CN	Carbon number
CNP	Carbon atoms inside the pore
E	Energy (kJ mol^{-1})
F	Molar flow rate (mol s^{-1})
H	Henry's coefficient (mol kg_{cat}^{-1} Pa^{-1})
H	Enthalpy (kJ mol^{-1})
h	Planck's constant
K_{deh}	Equilibrium coefficient for dehydrogenation (Pa)
$K_{isom}(O_{ij}, O_r)$	Equilibrium coefficient for isomerization between alkene j and reference alkene (–)
K_L	Langmuir physisorption coefficient (Pa^{-1})
K_{pm}	Equilibrium constant for pore mouth physisorption (Pa^{-1})
$K_{pm\text{-}mp}$	Equilibrium constant for pore mouth to micropore physisorption (moles in micropores/moles in pore mouth)
$K_{prot}^{usy}(O_{ij}, m)$	Equilibrium coefficient for protonation of alkene j with formation of a carbenium ion of type m (kg_{cat} mol^{-1}) on USY
$K_{prot}^{zsm\text{-}22}(O_{ij}, m)$	Equilibrium coefficient for protonation of alkene j with formation of a carbenium ion of type m on ZSM-22 (mol_{pm} mol^{-1})
$k(m, n)$	Rate coefficient of a reaction converting a carbenium ion of type m into another carbenium ion of type n (s^{-1})
k_B	Boltzmann constant
m_1	Reactant carbenium ion (secondary or tertiary)
m_2	Product carbenium ion (secondary or tertiary)
n	Carbenium ion type (secondary or tertiary)
nob	Number of observations
nresp	Number of responses
N	Number of components
O_{ij}	Alkene j produced from alkane j
p_i	Partial pressure of component i (Pa)
R	Net production rate (mol kg_{cat}^{-1} s^{-1})
$r(m, n)$	Rate of reaction converting reactant carbenium ion of type m into product carbenium ion of type n (mol kg_{cat}^{-1} s^{-1})
S	Entropy (J mol^{-1} K^{-1})
T	Temperature (K)
nole	Number of alkenes
ncar	Number of carbenium ions

7.2. Greek symbols

β	Beta scission
σ	Global symmetry number
Δ	Differential

7.3. Superscript

o	Standard state
$\sim$	Single event
comp	Composite
comp-ZSM-22	Composite for ZSM-22
comp-USY	Composite for USY
m	Modes of physisorption index
phys	Physisorption
sat	Saturation
trans	Translational
$\neq$	Transition state
deh	Dehydrogenation
prot	Protonation
rot	Rotational
i	Component index

7.4. Subscript

act	Activation
act-pcp/β	Activation for pcp, or β-scission reactions
as/pcp/β	Alkyl shifts, pcp, or β-scission reactions
Br	Branches
CNP	Carbon atoms inside the pore
cd	Charge delocalization
deh	Dehydrogenation
i, rot	Internal rotation
i	Component index
isom	Isomerization
j	Component index
k	Component index
m	Modes of physisorption index
me	Methyl group and carbon atom carrying methyl group
$O_{i,j}$	Alkene j stemming from alkane i
p	Index for alkanes
phys	Physisorption
pm	Pore mouth
pm-mp	Pore mouth to micropore
prot	Protonation
prot-acidity	Effect on protonation due to acidity
prot-CN	Effect on protonation due to carbon number dependency
r	Component index
R_{ik}^{+}	Carbenium ion k stemming from alkane i
t	Total

Acknowledgments

This research has been done as a part of the Interuniversitaire attractiepolen (IAP), funded by the Belgian government, Diensten van de Eerste Minister-Federale diensten voor wetenschappelijke, technische en culturele aangelegenheden.

References

[1] J.A. Martens, P.A. Jacobs, in: E.G. Derouane, et al. (Eds.), Zeolite Microporous Solids: Synthesis, Structure and Reactivity, 1992, p. 511.
[2] P.B. Wiesz, Pure Appl. Chem. 52 (1980) 2091.
[3] A. Corma, Catal. Lett. 22 (1993) 33.
[4] I.E. Maxwell, W.H.J. Stork, in: H. Van Bekkum, E.M. Flanigen, J.C. Lansen (Eds.), Introduction to Zeolite Science and Practice, Vol. 58, Elsevier, Amsterdam, 1991, p. 571.
[5] K.W. Smith, W.C. Starr, N.Y. Chen, Oil Gas J. 78 (21) (1980) 75.
[6] J.A. Ward, Fuel Process Technol. 35 (1993) 55.
[7] N.Y. Chen, W.E. Garwood, F.G. Dwyer, Shape Selective Catalysis in Industrial Applications, Dekker, New York, 1989.
[8] C. Marcilly, E. Benazzi, G. Marchal, Nathalie, US patent 6,198,015, 2001.
[9] M.A. Luengo, M. Yates, J. Mater. Sci. 30 (1995) 4483.
[10] Atlas of zeolite frame work types: http://www.iza-structure.org/databases/.
[11] J.A. Martens, W. Souverijns, W. Verrelst, R. Parton, G.F. Froment, P.A. Jacobs, Angew. Chem. Int. Ed. Engl. 34 (1995) 2528.
[12] W. Souverijns, J.A. Martens, G.F. Froment, P.A. Jacobs, J. Catal. 174 (1998) 177.
[13] M.C. Claude, PhD thesis, L'Universite Pierre et Marie Curie & Katholieke Universiteit Leuven, 1999.
[14] M.C. Claude, J.A. Martens, J. Catal. 190 (2000) 39.
[15] M.C. Claude, G. Vanbutsele, J.A. Martens, J. Catal. 203 (2001) 213.
[16] K.-C. Park, S.-K. Ihm, Appl. Catal. A 203 (2000) 201.
[17] L.M.Th. Maesen, M. Schenk, T.J.H. Vlugt, J.P. De Jonge, B. Smit, J. Catal. 188 (1999) 403.
[18] L.M.Th. Maesen, M. Schenk, T.J.H. Vlugt, J.P. De Jonge, B. Smit, J. Catal. 203 (2001) 281.
[19] J.A. Martens, G. Vanbutsele, P.A. Jacobs, J. Denayer, R. Ocakoglu, G. Baron, J.A. Munoz Arroyo, J.W. Thybaut, G.B. Marin, Catal. Today 65 (2001) 111.
[20] S. Ernst, J. Wietkamp, J.A. Martens, P.A. Jacobs, Appl. Catal. A 48 (1989) 137.
[21] J.A. Martens, R. Parton, L. Uytterhoeven, P.A. Jacobs, Appl. Catal. 76 (1991) 95.
[22] J.A. Munoz Arroyo, G.G. Martens, G.F. Froment, G.B. Marin, P.A. Jacobs, J.A. Martens, Appl. Catal. A 192 (2000) 9.
[23] R. Parton, L. Uytterhoeven, J.A. Martens, P.A. Jacobs, Appl. Catal. 76 (1991) 131.
[24] W. Souverijns, J.A. Martens, L. Uytterhoeven, G.F. Froment, P.A. Jacobs, Stud. Surf. Sci. Catal. 105 (1997) 1285.
[25] J.F.M. Denayer, PhD thesis, Vrije Universiteit Brussels, 1998.
[26] van de Runstraat, J.A. Kamp, P.J. Stobbelaar, J. van Grondelle, S. Krijnen, R.A. van Santen, J. Catal. 171 (1997) 77.
[27] C.S. Laxmi Narasimhan, J.W. Thybaut, G.B. Marin, J.A. Martens, J.F. Denayer, G.V. Baron, J. Catal. 218 (2003) 135.
[28] J.F.M. Denayer, G.V. Baron, P.A. Jacobs, J.A. Martens, J. Phys. Chem. B 102 (17) (1998a) 3077.
[29] J.F.M. Denayer, G.V. Baron, W. Souverijns, J.A. Martens, P.A. Jacobs, J. Phys. Chem. B 102 (23) (1998b) 4588.
[30] J.F. Denayer, G.V. Baron, G. Vanbutsele, P.A. Jacobs, J.A. Martens, Chem. Eng. Sci. 54 (1999) 3553.
[31] R.A. Ocakoglu, J.F.M. Denayer, G.B. Marin, J.A. Martens, G.V. Baron, J. Phys. Chem. B 107 (1) (2003) 398.
[32] P.B. Weisz, Adv. Catal. 13 (1962) 137.
[33] H.L. Coonradt, W.E. Garwood, Ind. Eng. Chem., Process. Des. Dev. 3 (1964) 38.
[34] M. Schenk, B. Smit, T.J.H. Vlugt, Th.L.M. Maesen, Angew. Chem. Int. Ed. 40 (2001) 736.
[35] P. Meriaudeau, A. Tuan Vu, F. Lefebvere, V.T. Nghiem, C. Naccache, Micropor. Mesopor. Mater. 22 (1998) 435.
[36] V.T. Ngheim, G. Sapalay, P. Mereaudeau, C. Naccache, Top. Catal. 14 (2001) 131.
[37] W. Zhang, P.G. Smirniotis, J. Catal. 182 (1999) 400.

[38] S.A. Quader, S. Singh, W.H. Wiser, G.R. Hill, J. Inst. Petrol. 56 (550) (1970) 187.
[39] B.E. Stangeland, Ind. Eng. Chem. Process. Des. Dev. 13 (1) (1974) 72.
[40] R.J. Quann, S.B. Jaffe, Ind. Eng. Chem. Res. 31 (1992) 2483.
[41] R.J. Quann, S.B. Jaffe, Chem. Eng. Sci. 51 (1995) 1615.
[42] D. Browarzik, H. Kehlen, Chem. Eng. Sci. 49 (1994) 923.
[43] C.S. Laxminarasimhan, R.P. Verma, P.A. Ramachandran, AIChE J. 42 (1996) 2645.
[44] M.A. Baltanas, K.K. Van Raemdonck, G.F. Froment, S.R. Mohedas, Ind. Eng. Chem. Res. 28 (1989) 899.
[45] E. Vynckier, G.F. Froment, in: G. Astarita, S.I. Sandler (Eds.), Kinetic and Thermodynamic Lumping of Multicomponent Mixtures, Elsevier, Amsterdam, 1991, p. 131.
[46] G.G. Martens, G.B. Marin, J.A. Martens, P.A. Jacobs, G.V. Baron, J. Catal. 195 (2000) 253.
[47] J.W. Thybaut, G.B. Marin, G.V. Baron, P.A. Jacobs, J.A. Martens, J. Catal. 202 (2001) 324.
[48] G.G. Martens, PhD thesis, Ghent University, 2000.
[49] G.F. Froment, K.B. Bischoff, Chemical Reactor Analysis and Design, 2nd ed., Wiley, New York, 1990.
[50] NETLIB, http://www.netlib.now.edu.an.
[51] L. Petzold, Siam. J. Sci. Stat. Comput. 4 (1983) 136.
[52] D.W. Marquardt, J. Soc. Indust. Appl. Math. 11 (1963) 431.
[53] P.T. Boggs, R.H. Byrd, J.E. Rogers, R.B. Schnabel, NISTIR 92-4834, 1992.
[54] G.G. Martens, G.B. Marin, AIChE J. 47 (2001) 1607.
[55] S.W. Benson, F.R. Cruickshank, D.M. Golden, G.R. Haugen, H.E. O'Neal, A.S. Rodgers, R. Shaw, R. Walsch, Chem. Rev. 69 (1969) 279.
[56] G.G. Martens, J.W. Thybaut, G.B. Marin, Ind. Eng. Chem. Res. 40 (2001) 1832.